Electronic Supplementary Information

Axially Chiral Bay-Tetraarylated Perylene Bisimide Dyes as Non-Fullerene Acceptors in Organic Solar Cells

Bernhard Mahlmeister,[a] Rebecca Renner,[b] Olga Anhalt,[a] Matthias Stolte,[ab] Frank Würthner[ab]*

[a] Universität Würzburg, Center for Nanosystems Chemistry (CNC), Theodor-Boveri-Weg, 97074 Würzburg, Germany

[b] Universität Würzburg, Institut für Organische Chemie, Am Hubland, 97074 Würzburg, Germany

*E-mail: wuerthner@uni-wuerzburg.de

Table of Contents

1. Materials and Methods

All chemicals, reagents and solvents were purchased from commercial suppliers and used after appropriate purification if not stated otherwise. *N*,*N'*-di(2,6-diisopropylphenyl)-1,6,7,12-tetrachloroperylene-3,4:9,10-bis(dicarboximides) and PBIs **1a**-**1e** as well as **2b**–**5b** were synthesized according to literature known procedures.[S1,S2] Toluene used for synthesis was of HPLC grade and was dried prior to use utilizing a *Pure Solv MD 7* system from *Inert Technology*. Dichloromethane (DCM) was distilled prior to use. Column chromatography was performed using commercial glass columns packed with silica gel 60 M (particle size of 0.04-0.063 mm from Merck KGaA) stationary phase. Normal phase HPLC was performed on a *JASCO* recycling semipreparative HPLC system equipped with a *VP 250/21 NUCLEOSIL* 100-7 column from Macherey-Nagel. For chiral separation a *ReproSil 100 Chiral-NR 8 µm* column from Trentec (**1a**-**1e** as well as **2b**–**5b**) or *ReproSil Chiral-MIF 10 µm* column from Dr. Maisch (**2e** attempted) was utilized.

UV/Vis/NIR spectroscopy was carried out at room temperature on a Jasco V770 spectrophotometer. Solution spectra were taken using 10 mm cuvettes (SUPRASIL®, Hellma® Analytics, DCM spectroscopic grade). For thin-film spectra, the same spectrometer with an integration sphere was used. Neat films were prepared on quartz substrates (SUPRASIL®, Hellma® Analytics) from a chloroform solution (spectroscopic grade). Spectra of blend films were taken using the respective thin-film device.

Fluorescence spectroscopy was carried out on a *FLS980* fluorescence spectrometer from Edinburgh Instruments. Spectra were corrected against the photomultiplier sensitivity and the lamp intensity. Fluorescence quantum yields were determined using the dilution method (OD < 0.05) and Oxazine 1 in ethanol with 11% as reference.[S3]

Fluorescence lifetimes were determined with EPL picosecond pulsed diode lasers (λ_{ex} = 560 nm) for time correlated single photon counting.

CD spectroscopy was carried out using a customised *JASCO CPL-300/J-1500* hybrid spectrometer.

NMR spectroscopy was performed using a Bruker *Avance III HD* 400 MHz NMR spectrometer relative to residual undeuterated solvent signals. Chemical shifts (δ) are listed in parts per million (ppm). The multiplicities for proton signals are abbreviated as *d* and *bm* for doublet and broad multiplet, respectively.

High resolution mass spectra were measured by electron spray ionization (**ESI**) using an *ESI microTOF Focus* mass spectrometer from Bruker Daltonics GmbH.

Melting points were determined using a SMP50 from *Stuart Equipment*.

Cyclic Voltammetry was measured on an *EC epsilon* (BASi instruments, UK) potentiostat connected with a three-electrode single-compartment cell. A platinum disc electrode was utilized as working electrode, a platinum wire as counter electrode and an Ag/AgCl electrode as reference electrode.

Single crystal X-ray diffraction was measured on a Bruker *D8 Quest Kappa* diffractometer with a Photon II CMOS detector and multi-layered mirror monochromated $Cu_{K\alpha}$ radiation at 100 ± 1 K. The solved structures were obtained with Fourier techniques and the *Shelx* software package.[S4] Crystallographic data are deposited on the Cambridge Crystallographic Data Centre as supplementary publication no. CCDC 2106434 (*Rac*-**1b**), CCDC 2106433 (*P*-**1b**), CCDC 2106436 (*Rac*-**1e**), CCDC 2106435 (*M*-**1e**) and CCDC 2106437 (*Rac*-**2e**).

AFM-Images were obtained by *NT-MDT Next Solver System* in semi contact mode by using a SCOUT 350 RAI (Nu Nano Ltd) silicon cantilever (spring constant = 42 N m^{-1}, resonance frequency = 350 kHz).

Organic thin-film devices (OSCs, SCLC) were prepared as organic solar cells in inverted bulk-heterojunction structure of ITO/ZnO/Blend/MoO_3/Al. SCLC-devices were fabricated in a structure of ITO/ZnO/Blend/BCP/Al (electron-mobility) or ITO/PEDOT:PSS/Blend/MoO_3/Al (hole mobility).

ITO-substrates (Soluxx GmbH) were cleaned with acetone (VWR, semiconductor grade), detergent, deionized water, and isopropanol (VWR, semiconductor grade) for 15 min each, followed by an ozone/UV treatment for 30 min.

The bottom layer was either ZnO or PEDOT:PSS. The ZnO-layer was deposited by static spin-casting ZnO nanoparticles[S5] on top of the substrates (3000 rpm, 30 s) followed by thermal annealing (200 °C, 1 h). PEDOT:PSS (solids content: 1.3 – 1.7%, PEDOT:PSS 1:6 w/w, Heraeus) was deposited analogously by spin-casting with 2500 rpm for 60 s and thermally annealing at 150 °C for 10 min.

The donor-acceptor blends were prepared by stirring a **PCE-10** (1-Material Inc.) polymer solution overnight in chlorobenzene (CB). This solution was then given to the respective PBI and stirred for 4 h at room temperature under inert conditions followed by dynamic spin-casting at 1000 rpm for 60 s (MBraun Intergas Systeme GmbH, UNIlab Pro, $c(O_2) < 1$ ppm, $c(H_2O) < 1$ ppm).

For vaccum deposition, the substrates were placed in the evaporation system (OPTIvap-XL, Creaphys GmbH). As top layers, either MoO_3 or BCP (d = 10 nm, r = 0.07 – 0.15 Å s^{-1}, $p < 10^{-6}$ mbar, rotation = 10 rpm) were deposited followed by aluminium (d = 100 nm, r = 1 - 2 Å s^{-1}, $p < 10^{-6}$ mbar) using shadow masks.

The device area was 7.1 mm^2. *J-V*-characteristics were measured after calibration with

a standard silicon solar cell with a KG filter (ISE Freiburg) under an AM1.5G *Oriel Sol3ATM* Class AAA solar simulator (Newport®) by a parameter analyser (Botest Systems GmbH).

SCLC measurements were recorded and evaluated using the protocol of Blakesley *et al.*[S6] applying Mott-Murgatroyd equation and a built-in-voltage of $V_{bi} = 0.6$ V (**PCE-10**, **1b**) and a relative permittivity of $\varepsilon = 3.5$. Active layer thickness was determined *via* AFM.

***EQE* measurements** were carried out with a Quantum Efficiency/IPCE measurement kit (Newport®) by using a 300 W Xe-lamp and a Cornerstone monochromator with a Merlin Lock-In Amplifier for detection.

TD-DFT calculations were performed with GAUSSIAN 09 software[S7] on wB97/def2SVP level of theory. Molecule coordinates were taken from respective single-crystal structures without further geometry optimization.

2. Synthesis

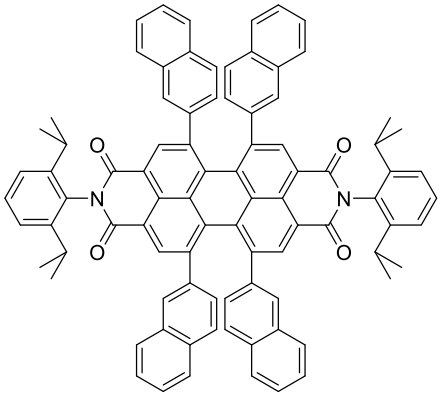

2e

N,*N*′-di(2,6-diisopropylphenyl)-1,6,7,12-tetrachloroperylene-3,4:9,10-bis(dicarboximide) (100 µmol), 2-naphthylboronic acid (2.00 mmol, 20 eq.), anhydrous potassium carbonate (145 mg, 1.05 mmol, 10.5 eq.) and tetrakis(triphenylphosphine)palladium (34.7 mg, 30.0 µmol, 0.3 eq.) were given in a Schlenk tube. Degassed toluene (3.2 mL), ethanol (0.6 mL) and water (1.6 mL) were added. The mixture was subjected to three freeze-pump-thaw cycles. After stirring for 26 h at 80 °C, the mixture was extracted with dichloromethane and washed three times with water. The organic phases were combined, and the solvent removed under reduced pressure. The crude product was purified by column chromatography (hexane:dichloromethane 3:7) and HPLC (hexane:dichloromethane 1:2) to obtain 45.5 mg (37.4 mmol, 37%) of **2e** as purple solid.

^{1}H-NMR (400 MHz, CD_2Cl_2, 293 K): δ = 8.54 – 6.68 (bm, 38H), 2.91 (bm, 4H), 1.26 (d, 12H), 1.16 (d, 12H);

^{13}C-NMR (100 MHz, CD_2Cl_2, 293 K): δ = 164.4, 146.6, 143.2, 138.4, 134.9, 132.9, 132.6, 132.4, 131.7, 129.9, 128.5, 128.2, 127.9, 127.5, 127.0, 126.6, 124.5, 122.9, 29.5, 24.2;

HRMS (ESI-TOF, pos. mode, MeCN/$CHCl_3$): *m/z* calculated for $C_{88}H_{66}N_2NaO_4^+$ $[M+Na]^+$: 1237.4915, found 1237.4877; m.p. >390 °C.

UV/Vis (CD_2Cl_2): λ_{max} / nm (ε / M^{-1} cm^{-1}) = 615 (23900), 536 (25300).

Fluorescence (CD_2Cl_2, λ_{ex} = 600 nm): λ_{max} / nm (ϕ_f / %) = 670 (31),

τ / ns (λ_{ex} = 560 nm): = 9.3.

m.p.: >390 °C.

3. UV/Vis/NIR and Fluorescence

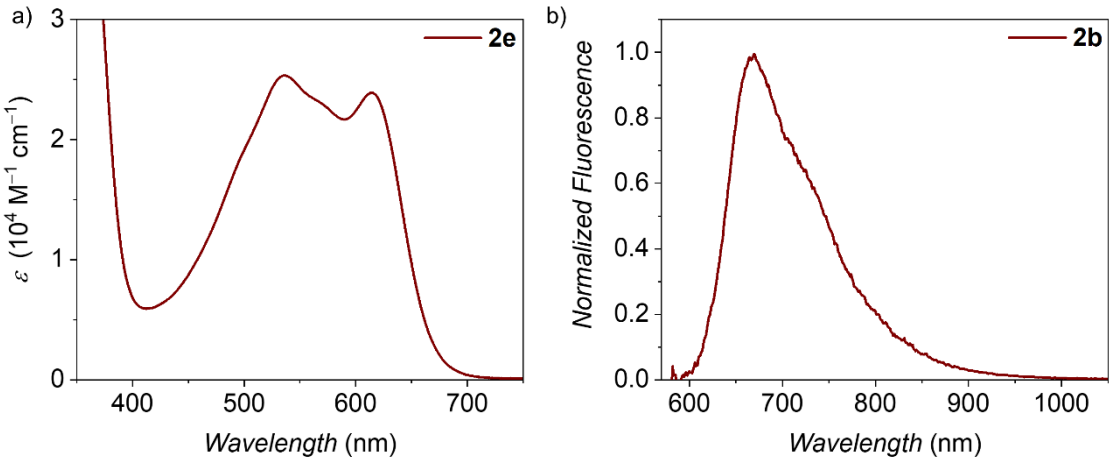

Fig. S1 a) UV/Vis/NIR absorption spectra of **2e** and b) normalized emission spectra in DCM solution ($c_0 \approx 4 \cdot 10^{-6}$ M) at room temperature.

4. OPV

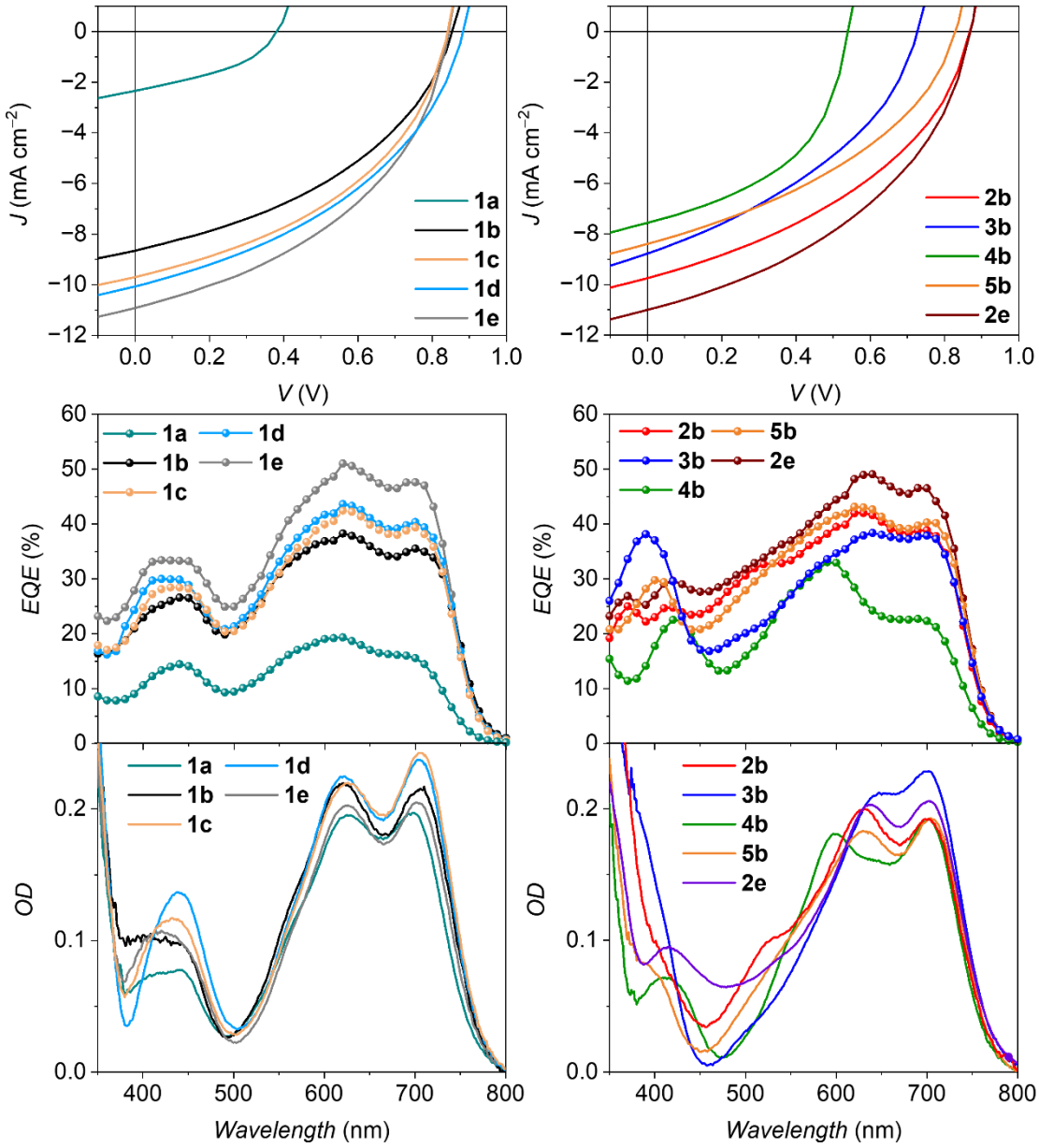

Fig. S2 *J-V* characteristics (upper figures) as well as *EQE* (middle figures) and UV/Vis/NIR absorption spectra (lower figures) of **PCE-10** based devices of **1a**–**1e** (left) as well as **2b**–**5b** and **2e** (right). The total blend concentration was 15 mg ml^{-1} (16 mg ml^{-1} for **2e**) in chlorobenzene (CB) for all devices. D:A ratio was 1:1 (1.0:1.1 for **2e**) and 2% of 1-Chloronaphthalene (CN) was used as solvent additive. The solar cells were fabricated and characterized under inert conditions and AM1.5 G irradiation.

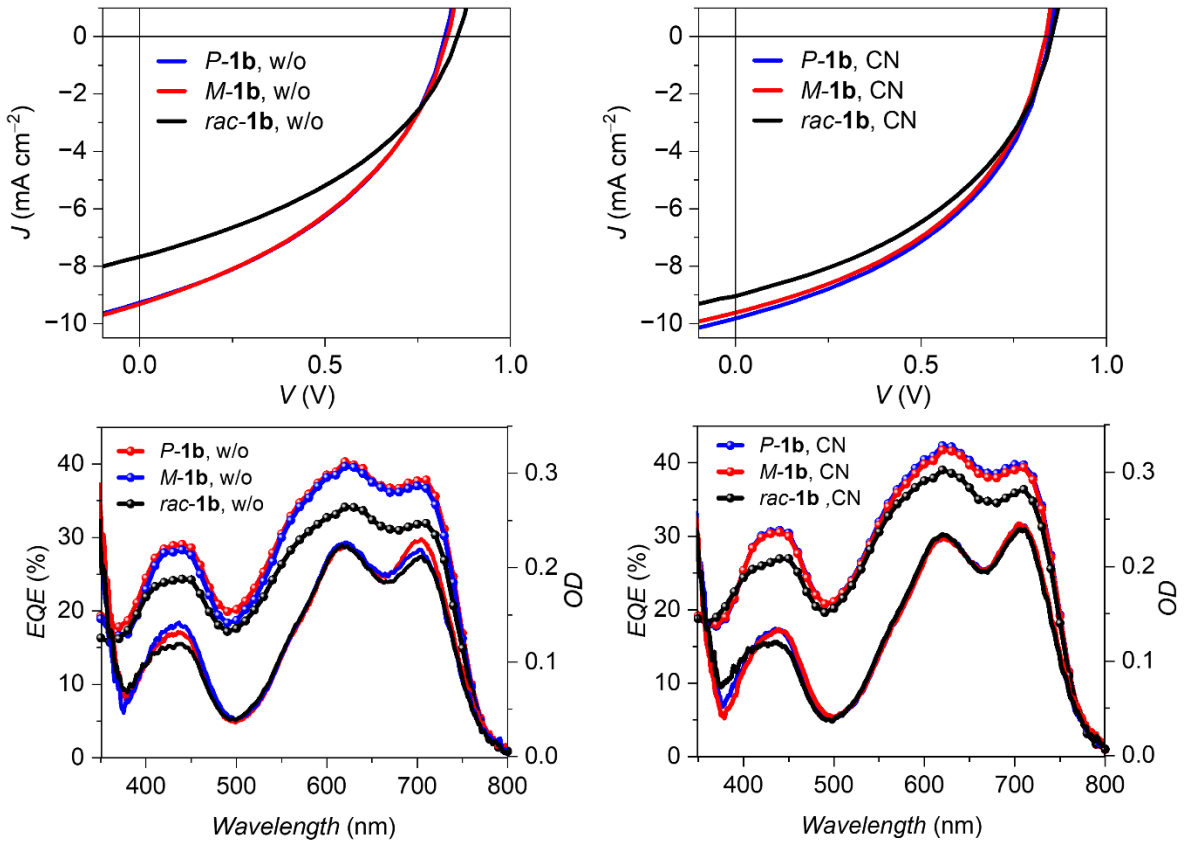

Fig. S3 *J-V* characteristics (top) of best **1b** based OSC devices with inverted architecture of ITO/**PCE-10**:**1b**/MoO_3/Al without solvent additive (left) or with 2% of 1-Chloronaphthalene (CN, right). *EQE* and UV/Vis/NIR absorption spectra of respective devices (bottom). The solar cells were fabricated and characterized under inert conditions and AM1.5 G irradiation.

5. AFM

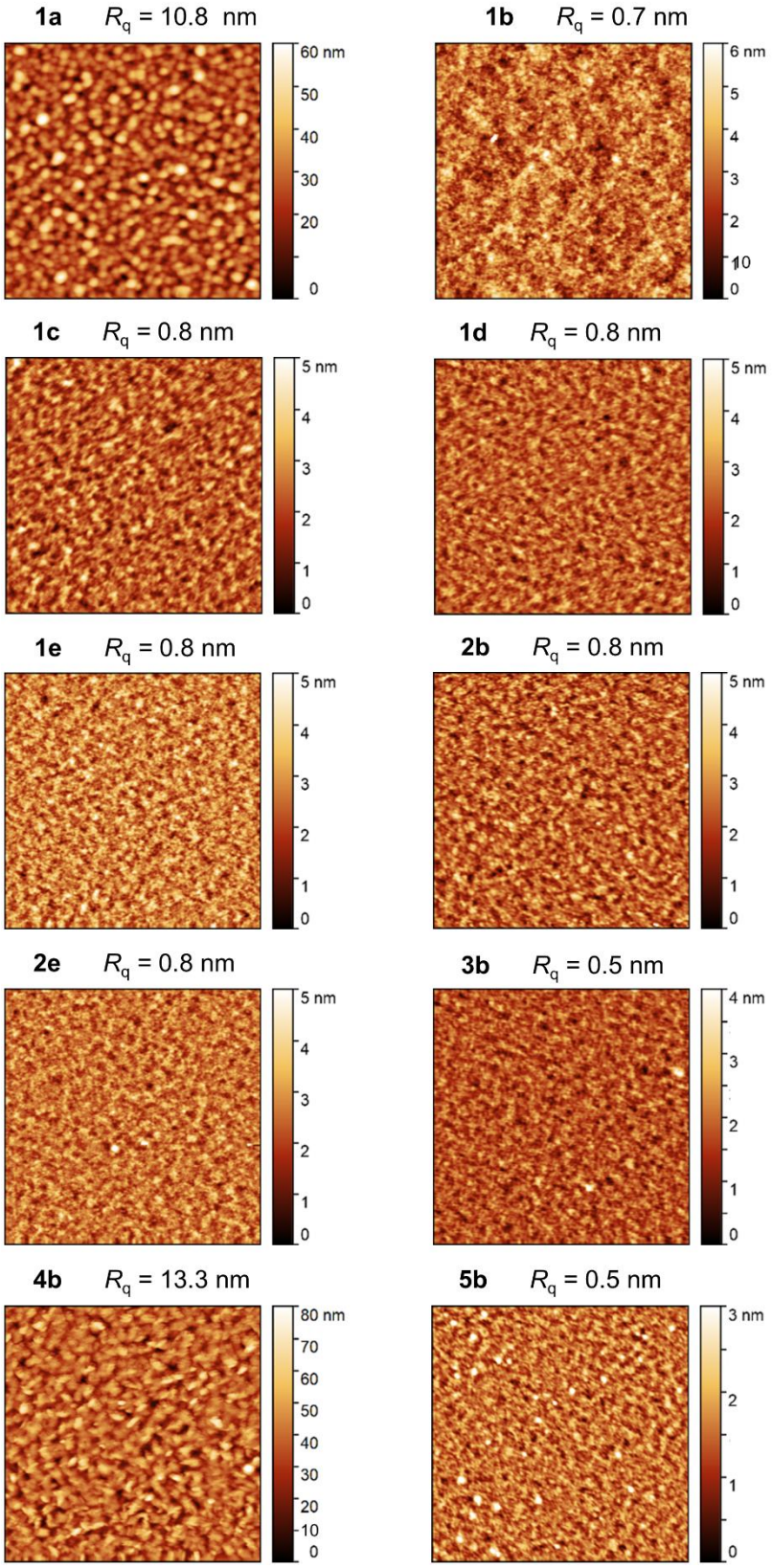

Fig. S4 AFM-height images of all **PCE-10** based PBI blends used as OSC device corresponding to Fig. 2 and Table 1. Thin film devices were spin-coated on ITO/ZnO coated glass substrate at room temperature under inert conditions. 5 x 5 μm^2.

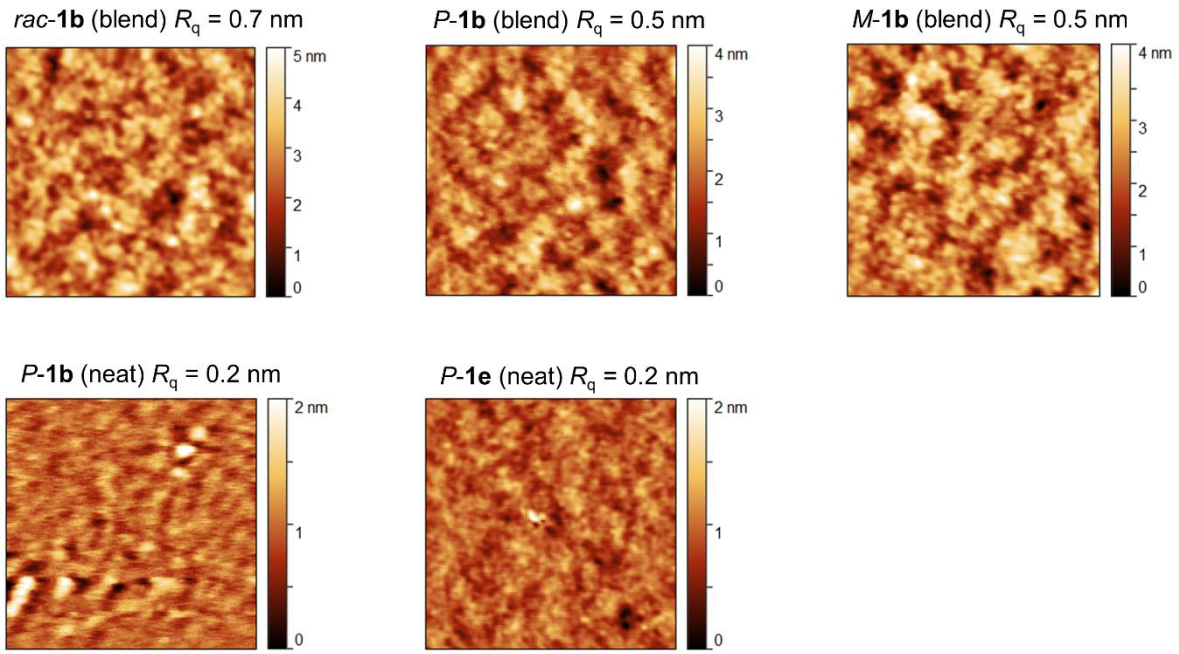

Fig. S5 AFM-height images of **PCE-10** based PBI blends of *P*/*M*/*Rac*-**1b** used as OSC device corresponding to Fig. 4 and Table 2 (top) as well as neat films of *P*-**1b** and *P*-**1e** from a chloroform solution (c = 10 mg ml^{-1}). Thin films were spin-coated on ITO/ ZnO coated glass substrate (blends) or quartz (neat films) at room temperature under inert conditions. 5 x 5 µm^2.

6. X-Ray

Table S1 X-ray structure characteristics for all tetraarylated PBI derivatives.

	Rac-**1b**	*Rac*-**1e**	*Rac*-**2e**	*P*-**1b**	*M*-**1e**
Empirical formula	$C_{57}H_{43}Cl_{13}N_2O_4$	$C_{79}H_{68}Cl_{12}N_2O_4$	$C_{100}H_{76}Cl_{12}N_2O_4$	$C_{57}H_{43}Cl_{12}N_2O_4$	$C_{76}H_{60}Cl_{16}N_2O_4$
$M_{empirical}$ (g mol^{-1})	926.28	1523.08	1440.52	888.08	1253.94
Wavelength (Å)	1.54178	1.54178	1.54178	1.54178	1.54178
T (K)	100	100	100	100	100
Description of the crystal					
Color	Red	Red	Red	Red	Red
Habit	Needle	Needle	Needle	Needle	Needle
Crystal System	Triclinic	Triclinic	Monoclinic	Hexagonal	Monoclinic
Space group	$P\bar{1}$	$P\bar{1}$	$P2_1/c$	$P6_522$	$P2_1$
Unit cell dimension					
a (Å)	12.4343(7)	12.5786(9)	15.5844(10)	19.1064(9)	14.0489(10)
b (Å)	12.6105(7)	16.3365(12)	29.7802(17)	19.1064(9)	13.8721(10)
c (Å)	16.4663(10)	18.8231(14)	17.1937(10)	44.020(2)	16.7450(12)
α (°)	101.657(3)	74.006(3)	90	90	90
β (°)	90.456(3)	87.132(3)	110.767(3)	90	109.392(3)
γ (°)	118.044(3)	87.033(3)	90	120	90
Volume (Å^3)	2215.9(2)	3710.7(5)	7461.3(8)	13916.8(15)	3078.3(4)
Z	2	2	4	12	2
$\rho_{alc.}$ (g cm^{-3})	1.388	1.363	1.282	1.272	1.353
F(000)	964	1573	3024	5561.3	1304
Range of θ (°)	2.760 – 72.452	2.443 – 72.498	2.986 – 72.624	2.670 – 72.141	2.797 – 72.567
Goodness of Fit	1.027	1.019	1.052	1.116	1.088
CCDC	2106434	2106436	2106437	2106433	2106435

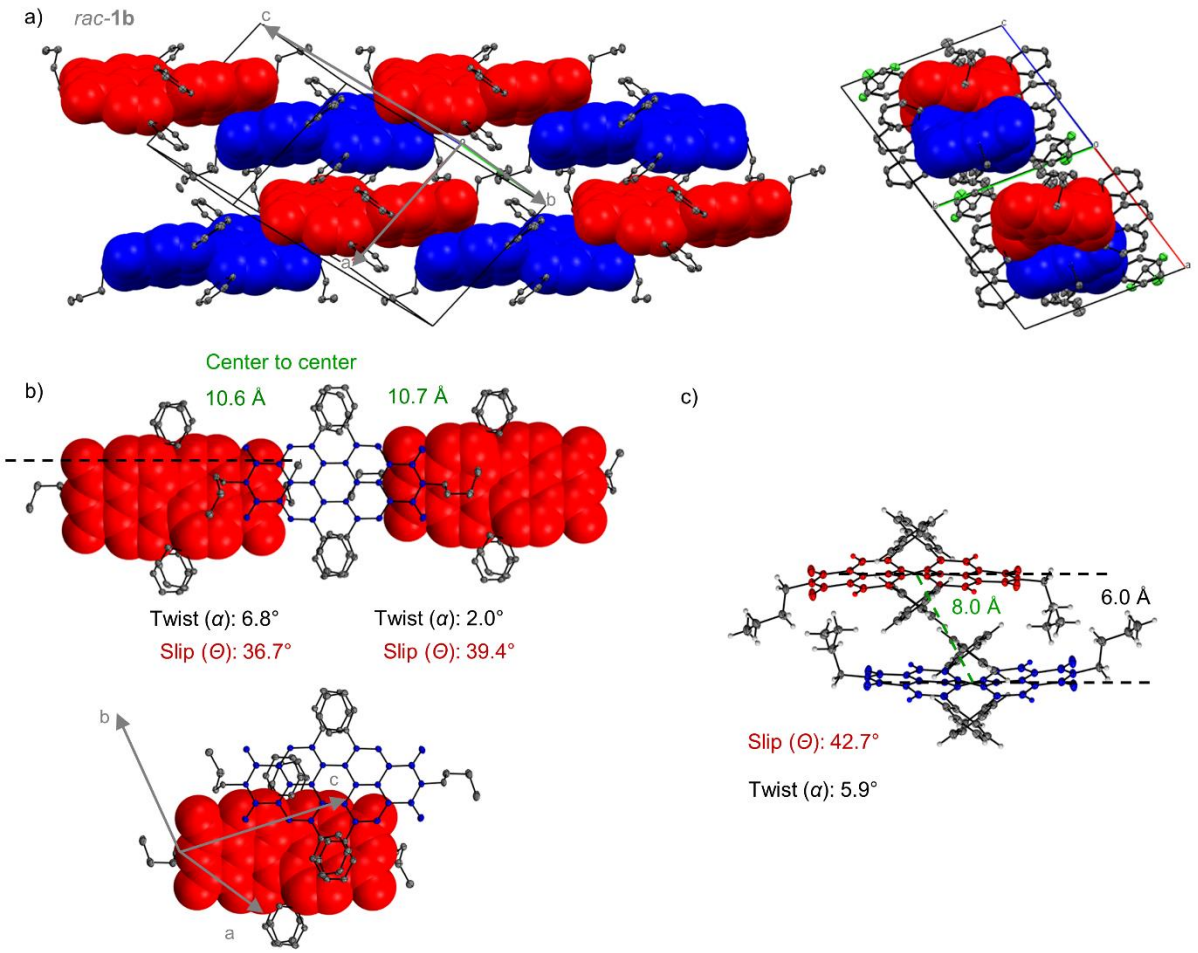

Fig. S6 a) Side view onto the unit cell of racemic PBI *rac*-**1b** (left) along the double stranded chromophore alignment within its single crystal structure (ellipsoids are set to 50 % probability) as well as rotated side view (right). (b). Top view onto the chromophore slip-stack arrangement of one isolated double strand (top) as well as top view onto a pair of enantiomers within the same unit cell (bottom). c) Rotated side view onto the chromophores within their unit cell. PBI atropo-enantiomers are colored in blue (*P*) and red (*M*), respectively. The ellipsoids are set to 50 % probability (C: gray). Disorder of the imide residues, hydrogen atoms as well as solvent molecules are omitted for clarity. The distance between the planes of adjacent chromophores (black) and distances between the centroids of the perylene cores (green), as well as twist angle α (black) and slip angle Θ (red) between two chromophores are indicated as well.

Table S2 Calculated Coulomb coupling between a *P*-**1b** atropo-enantiomer and its adjacent *M*-**1b** chromophores in either –*a*-axis or *c*-axis direction (Fig. S6b) within their racemic single crystal structure based on Kasha's molecular exciton theory.[S8]

rac-**1b**	$r_{c\text{-}c}$ (Å)	μ_{eg}[a] (D)	α (°)	Θ (°)	J_{coul} (cm^{-1})
P / *M*-**1b** (–*a*-axis direction)	10.6	6.4	6.8	39.4	–140.2
P / *M*-**1b** (*c*-axis direction)	10.7	6.4	2.0	36.7	–156.9

a) The transition dipole moment μ_g was calculated from UV/Vis/NIR absorption in DCM solution.

7. CD Spectroscopy

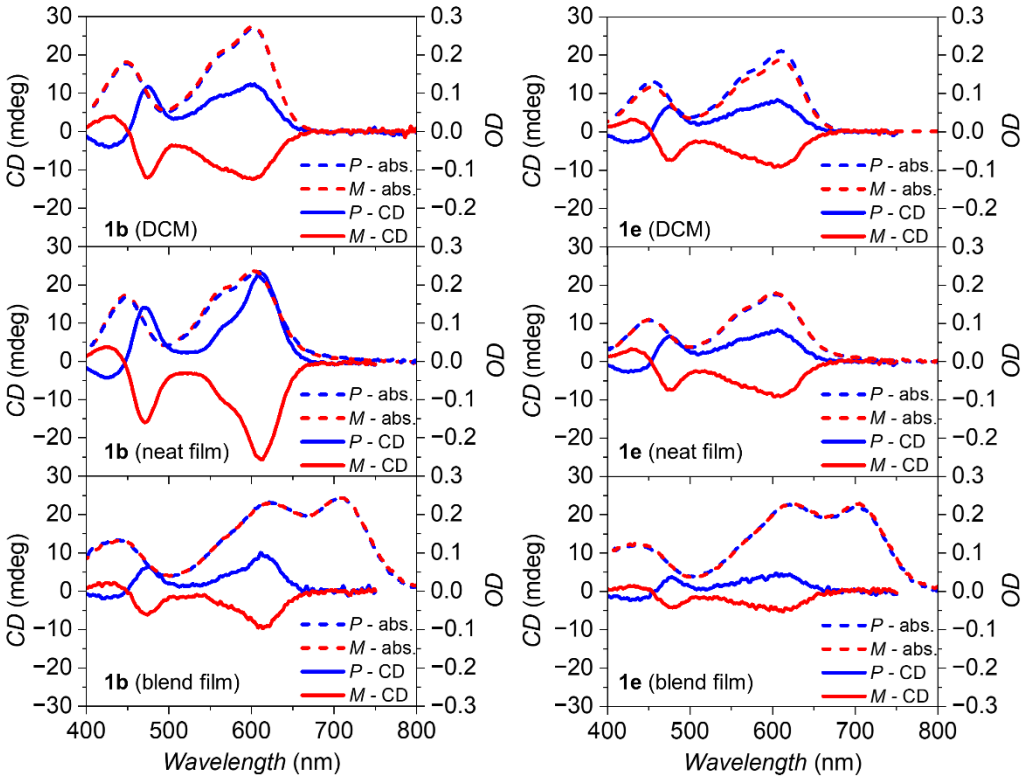

Fig. S7 UV/Vis/NIR absorption spectra (dashed lines) and CD spectra (solid lines) of *P*- (blue) and *M*- (red) atropo-enantiomers of **1b** (left) and **1e** (right). Spectra were taken in DCM solution (top) as well as spin coated neat film (center, from 10 mg ml^{-1} $CHCl_3$ solution on quartz) and OSC device (bottom, 15 mg ml^{-1} 1:1 **PCE-10**:PBI solution on ITO/ZnO).

8. SCLC

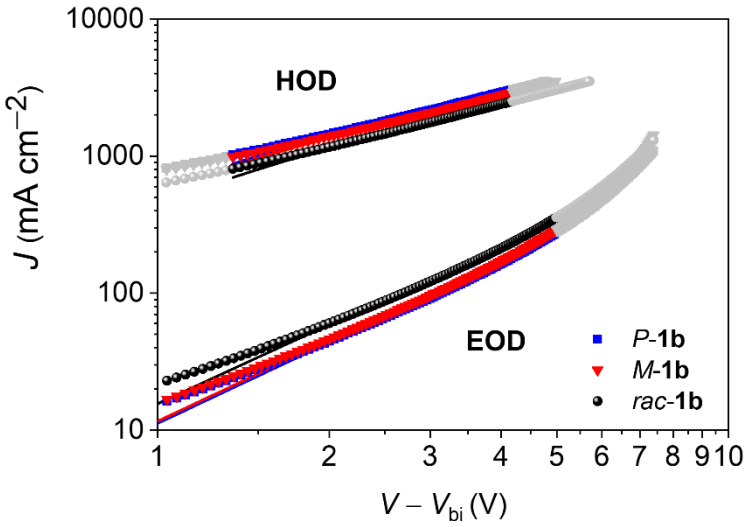

Fig. S8 *J-V* curves of PBI **1b** based SCLC devices including Mott-Murgatroyd fit. Electron only devices (EOD) and hole only devices (HOD) in structures of ITO/ZnO/**PCE-10**:PBI/BCP/Al (EOD) and ITO/PEDOT:PSS/**PCE-10**:PBI/MoO_3/Al (HOD) were fabricated and characterized under dark and inert conditions according to literature known procedure.[S6]

Table S3 Extracted hole mobilities and electron mobilities of **1b** based SCLC devices. Electron only devices (EOD) and hole only devices (HOD) in structure of ITO/ZnO/**PCE-10**:PBI/BCP/Al (EOD) and ITO/PEDOT:PSS/**PCE-10**:PBI/MoO_3/Al (HOD) were fabricated and characterized under dark and inert conditions according to literature known procedure.[S6]

Acceptor	$\mu_{electron}$[a] / $cm^2\ V^{-1}\ s^{-1}$	μ_{hole}[a] / $cm^2\ V^{-1}\ s^{-1}$	$\mu_{electron\ max}$ / $cm^2\ V^{-1}\ s^{-1}$	$\mu_{hole\ max}$ / $cm^2\ V^{-1}\ s^{-1}$
P-**1b**	$8.9 \pm 0.3 \cdot 10^{-6}$	$1.4 \pm 0.1 \cdot 10^{-3}$	$9.4 \cdot 10^{-6}$	$1.5 \cdot 10^{-3}$
M-**1b**	$9.1 \pm 0.4 \cdot 10^{-6}$	$1.3 \pm 0.1 \cdot 10^{-4}$	$9.7 \cdot 10^{-6}$	$1.4 \cdot 10^{-3}$
rac-**1b**	$13.7 \pm 0.2 \cdot 10^{-6}$	$1.0 \pm 0.1 \cdot 10^{-4}$	$13.9 \cdot 10^{-6}$	$1.1 \cdot 10^{-3}$

[a] Average of at least five independent devices.

9. TD-DFT

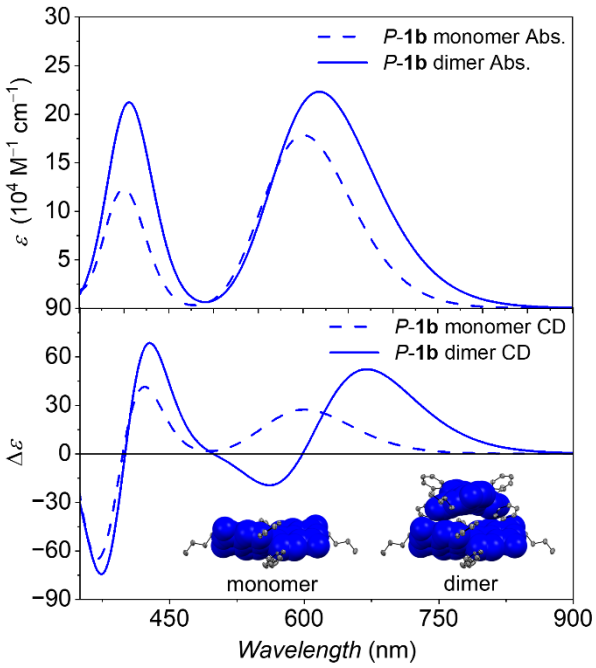

Fig. S9 TD-DFT calculated UV/Vis (top) and CD spectra (bottom) of *P*-**1b** monomer (dashed lines) and dimer (solid lines) using molecular geometry obtained from single crystal X-ray structure analysis. For monomer calculation, the bottom chromophore of the dimer entity with the lower twist angle of 32.4° was used (see inset or Fig.5). Calculations were performed on wB97/def2SVP level of theory and transition energies were shifted by 0.69 eV.

Table S4 Calculated UV/Vis/NIR transitions for monomeric *P*-**1b** (topmost molecule of the dimeric entity) obtained from its single crystal structure.

Transition	% Character	*Wavelength* (nm)	Oscillator strength
212 → 213	100	449.64	0.4395
194 → 213 204 → 213 210 → 213 211 → 214 212 → 217	2.9 4.3 78.9 5.6 8.3	333.15	0.0534
197 → 213 202 → 213 210 → 214 211 → 213 212 → 216	6.5 3.2 8.7 10.2 11.4	326.12	0.2503
204 → 213 210 → 213 212 → 215	63.2 2.7 31.1	305.04	0.0176
203 → 213 205 → 213 212 → 214	17.0 10.8 72.1	288.32	0.0105
195 → 215 197 → 213 198 → 214 198 → 228 199 → 213 199 → 219	3.1 11.0 30.0 4.3 45.5 6.2	275.62	0.0032
195 → 224 196 → 215 197 → 214 198 → 213 198 → 219 198 → 227 199 → 214 199 → 228	2.5 2.7 6.6 52.7 8.0 3.3 21.3 2.9	275.62	0.0003
203 → 213 203 → 216 204 → 213 205 → 216 210 → 214 210 → 229 212 → 215 212 → 227	3.2 2.7 3.2 2.4 7.8 2.4 7.7 70.6	266.17	0.0780
205 → 213 219 → 213 211 → 215 212 → 224	5.0 83.2 7.3 4.6	263.87	0.0012
204 → 213 205 → 216 210 → 214 210 → 229 212 → 215 212 → 227	9.6 4.9 7.2 7.0 31.7 39.5	263.06	0.6960

Table S5 Calculated UV/Vis/NIR transitions for dimeric *P*-**1b** obtained from its single crystal structure.

Transition	% Character	*Wavelength* (nm)	Oscillator strength
423 → 425	18.4	472.83	0.2182
424 → 425	23.9		
212 → 426	60.2		
423 → 425	58.9	451.64	0.3446
423 → 426	22.0		
424 → 425	9.7		
424 → 426	9.4		
419 → 425	2.6	342.65	0.0547
419 → 426	14.7		
421 → 428	3.4		
422 → 425	28.9		
422 → 426	45.4		
424 → 434	5.0		
419 → 425	42.3	336.21	0.0812
419 → 426	9.1		
422 → 425	24.7		
422 → 426	17.0		
423 → 433	6.9		
420 → 426	14.5	332.86	0.1447
421 → 425	20.8		
421 → 426	37.0		
422 → 428	5.0		
424 → 425	7.7		
224 → 426	3.6		
224 → 431	5.5		
224 → 232	6.0		
393 → 425	3.2	328.89	0.1444
419 → 427	3.2		
420 → 425	25.9		
420 → 426	8.4		
421 → 425	25.3		
221 → 426	9.0		
222 → 427	3.0		
223 → 231	5.1		
223 → 232	4.5		
224 → 225	8.3		
224 → 226	3.2		
420 → 225	6.8	324.80	0.0882
421 → 226	6.3		
424 → 225	58.7		
424 → 426	28.2		
223 → 425	23.5	312.12	0.0248
223 → 426	76.5		
401 → 425	3.2	310.16	0.0076
401 → 426	10.8		
407 → 426	3.9		
409 → 425	3.8		
409 → 426	10.0		
410 → 425	7.1		
410 → 426	6.9		
412 → 425	6.4		
412 → 426	10.5		
424 → 227	2.8		
424 → 229	14.0		
424 → 430	20.4		
401 → 425	5.3	306.80	0.0228
404 → 425	17.0		
404 → 426	5.9		
407 → 425	6.6		
410 → 425	12.4		
410 → 426	8.2		
412 → 426	2.8		
414 → 425	5.1		
423 → 427	3.2		
423 → 229	23.4		
423 → 230	10.1		

10. Cyclic Voltammetry

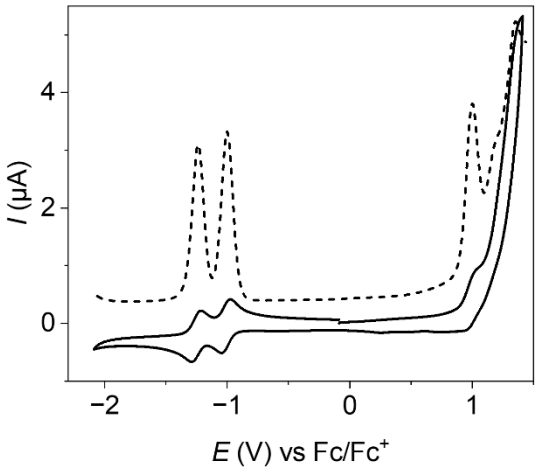

Fig. S10 Cyclic voltammograms (solid lines) as well as square wave voltammograms (dashed lines) of PBI **2e** in DCM solution ($c_0 \approx 2 \cdot 10^{-4}$ M) at 293 K using tetrabutylammonium hexafluorophosphat (TBAHFP 0.1 M) as electrolyte. The scanning speed was 100 mV s^{-1}.

Table S6 Redox properties of **2e**. Half-wave potentials were determined by square wave voltammetry measured in DCM (0.1 M TBAHFP) vs. Fc^+/Fc at room temperature.

PBI	E_{red1} (V)	E_{red2} (V)	E_{ox1} (V)	E_{HOMO}[a] (eV)	E_{LUMO}[a] (eV)	E_{gap} (eV)
2e	–1.00	–1.23	0.98	–6.13	–4.15	1.98

[a] Calculated according to literature known procedure using the experimentally determined redox potentials (E_{HOMO} = –[E_{ox1} + 5.15 eV] and E_{LUMO} = –[E_{red1} + 5.15 eV]) and the energy level of Fc+/Fc with respect to the vacuum level (–5.15 eV).[S9]

11. NMR Spectra

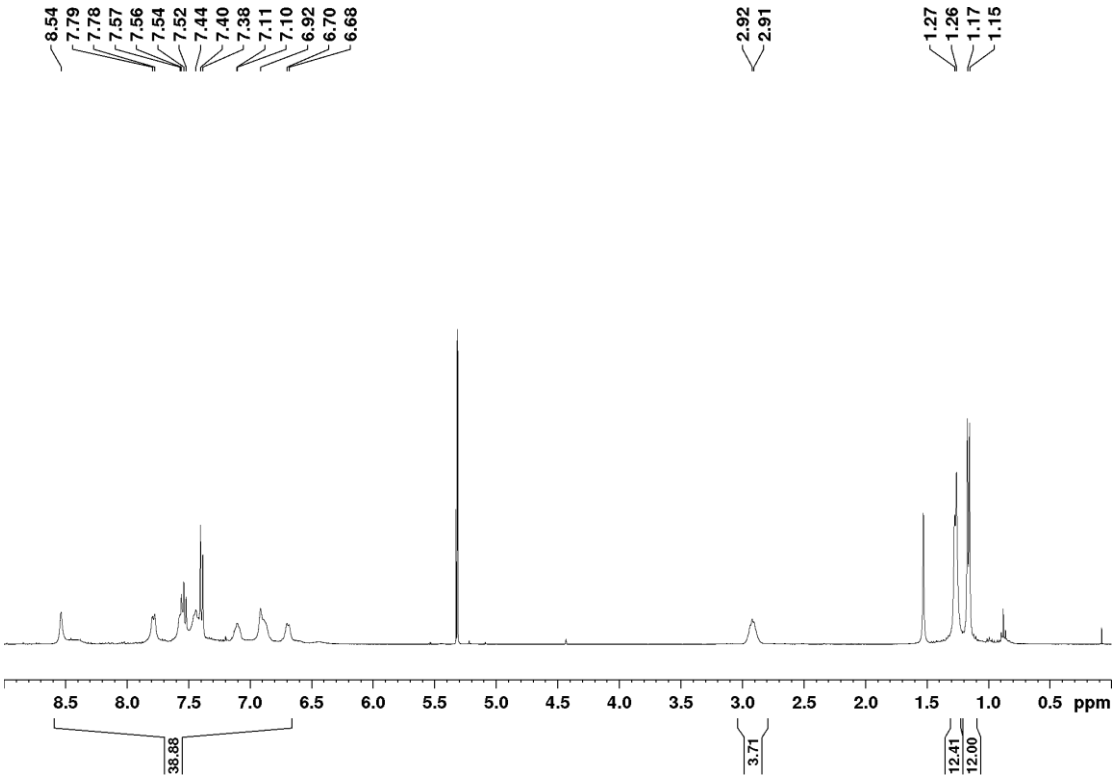

Fig. S11 ^{1}H NMR spectrum (400 MHz) of **2e** in CD_2Cl_2 at 298 K.

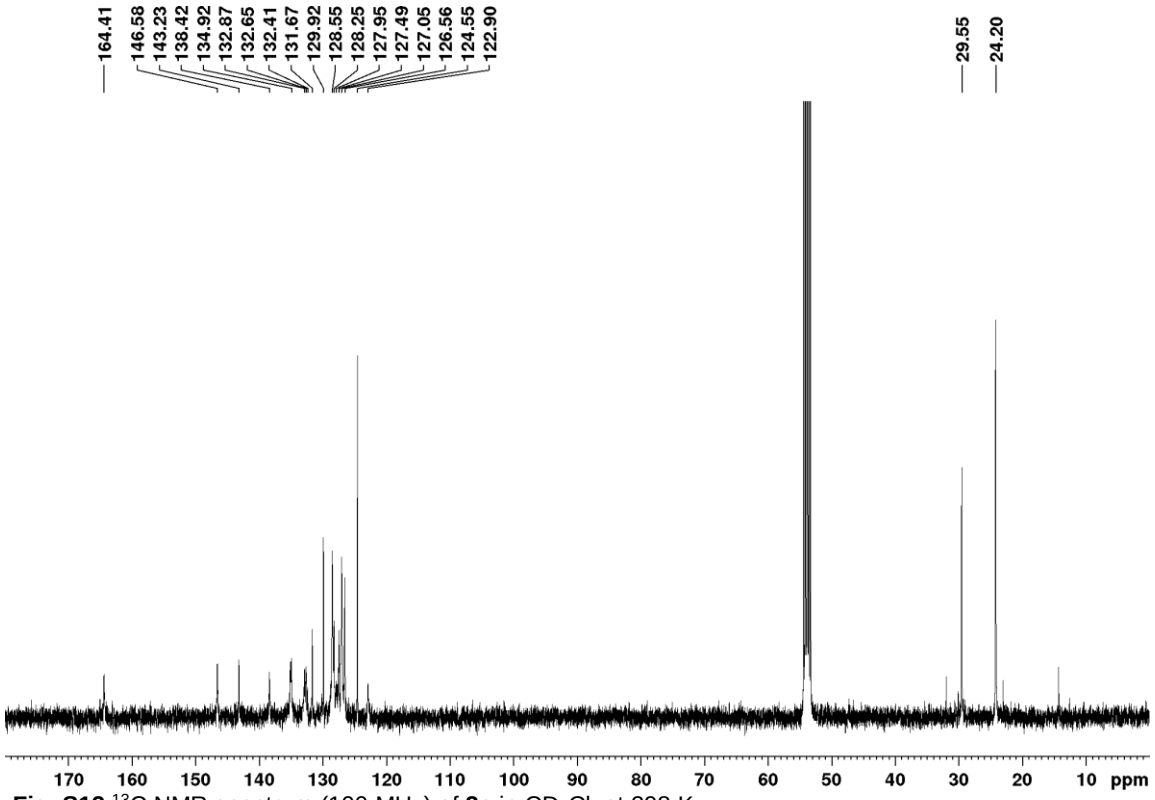

Fig. S12 ^{13}C NMR spectrum (100 MHz) of **2e** in CD_2Cl_2 at 298 K.

12. References

S1 a) F. Würthner, A. Sautter and J. Schilling, *J. Org. Chem.*, 2002, **67**, 3037–3044; b) B. Pagoaga, L. Giraudet and N. Hoffmann, Eur. *J. Org. Chem.*, 2014, 5178–5195.

S2 R. Renner, B. Mahlmeister, O. Anhalt, M. Stolte and F. Würthner, *Chem. Eur. J.*, 2021, accepted manuscript, **27**, /doi.org/10.1002/chem.202101877.

S3 R. Sens, K. H. Drexhage, *J. Lumin.*, 1981, **24**, 709–712.

S4 G. Sheldrick, *Acta Cryst. A*, 2008, **64**, 112–122.

S5 Y. Sun, J. H. Seo, C. J. Takacs, J. Seifter and A. J. Heeger, *Adv. Mater.*, 2011, **23**, 1679–1683.

S6 J. C. Blakesley, F. A. Castro, W. Kylberg, G. F. A. Dibb, C. Arantes, R. Valaski, M. Cremona, and J.-S. Kim, *Org. Electron.*, 2014, **15**, 1263–1272.

S7 M. J. Frisch, G. W. Trucks, H. B. Schlegel, G. E. Scuseria, M. A. Robb, J. R. Cheeseman, G. Scalmani, V. Barone, G. A. Petersson, H. Nakatsuji, X. Li, M. Caricato, A. V. Marenich, J. Bloino, B. G. Janesko, R. Gomperts, B. Mennucci, H. P. Hratchian, J. V. Ortiz, A. F. Izmaylov, J. L. Sonnenberg, Williams, F. Ding, F. Lipparini, F. Egidi, J. Goings, B. Peng, A. Petrone, T. Henderson, D. Ranasinghe, V. G. Zakrzewski, J. Gao, N. Rega, G. Zheng, W. Liang, M. Hada, M. Ehara, K. Toyota, R. Fukuda, J. Hasegawa, M. Ishida, T. Nakajima, Y. Honda, O. Kitao, H. Nakai, T. Vreven, K. Throssell, J. A. Montgomery Jr., J. E. Peralta, F. Ogliaro, M. J. Bearpark, J. J. Heyd, E. N. Brothers, K. N. Kudin, V. N. Staroverov, T. A. Keith, R. Kobayashi, J. Normand, K. Raghavachari, A. P. Rendell, J. C. Burant, S. S. Iyengar, J. Tomasi, M. Cossi, J. M. Millam, M. Klene, C. Adamo, R. Cammi, J. W. Ochterski, R. L. Martin, K. Morokuma, O. Farkas, J. B. Foresman and D. J. Fox, Wallingford, CT, 2016.

S8 M. Kasha, H. R. Rawls and M. A. El-Bayoumi, *Pure Appl. Chem.*, 1965, **11**, 371–393.

S9 A. Nowak-Król, K. Shoyama, M. Stolte and F. Würthner, *Chem. Commun.*, 2018, **54**, 13763–13772.